NASA TECHNICAL MEMORANDUM

UB
NASA TM X-1462

EXPERIMENTAL AND THEORETICAL AERODYNAMIC CHARACTERISTICS OF REPRESENTATIVE HYPERSONIC CRUISE CONFIGURATIONS

PART I. LIFT AND DRAG - *Walter P. Nelms, Jr.*
PART II. STABILITY AND TRIM - *John A. Axelson*

Ames Research Center
Moffett Field, Calif.

NATIONAL AERONAUTICS AND SPACE ADMINISTRATION • WASHINGTON, D. C. • OCTOBER 1967

~~CONFIDENTIAL~~

NASA TM X-1462

EXPERIMENTAL AND THEORETICAL AERODYNAMIC CHARACTERISTICS OF REPRESENTATIVE HYPERSONIC CRUISE CONFIGURATIONS

PART I. LIFT AND DRAG - Walter P. Nelms, Jr.

PART II. STABILITY AND TRIM - John A. Axelson

Ames Research Center
Moffett Field, Calif.

NATIONAL AERONAUTICS AND SPACE ADMINISTRATION

~~CONFIDENTIAL~~

EXPERIMENTAL AND THEORETICAL AERODYNAMIC CHARACTERISTICS OF REPRESENTATIVE HYPERSONIC CRUISE CONFIGURATIONS[1,2]

PART I. LIFT AND DRAG - Walter P. Nelms, Jr.

PART II. STABILITY AND TRIM - John A. Axelson

Ames Research Center

SUMMARY

Experimental results for three models representative of hypersonic cruise aircraft have been measured over a Mach number range from 0.65 to 7.4 and compared with various theoretical estimates for the supersonic and hypersonic speed ranges. The three different models were designed to the same general specifications for an air-breathing, liquid-hydrogen fueled, hypersonic cruise aircraft having a gross weight of approximately a half-million pounds and a wing area of 6250 square feet.

The basic models comprised of wing, body, and vertical tail, with nacelles removed, developed untrimmed hypersonic maximum lift-drag ratios near 4.2. Theoretical estimates of the lift characteristics generally agreed well with the experimental results. Less satisfactory agreement between theory and experiment resulted for the drag characteristics, however, primarily because of the underprediction of zero-lift drag at hypersonic speeds.

The longitudinal and directional aerodynamic centers and the aerodynamic performance are presented for the configuration buildups and for various degrees of stability and trim. Inviscid theoretical estimates of directional aerodynamic center were in fair agreement with experiment around a Mach number of 5 but inadequately accounted for the effects of increasing hypersonic Mach number where viscous interaction effects became dominant. The trimmed maximum lift-drag ratio at hypersonic Mach numbers for the models with rudders flared for directional stability and control was approximately 3.5.

INTRODUCTION

Recent studies of the potential of hydrogen-fueled hypersonic aircraft for both cruise and boost missions, as typified by reference 1, have indicated a need for research in the areas of theoretical prediction techniques and experimental testing procedures for these types of configurations. Theories are available for predicting hypersonic aerodynamic characteristics of relatively simple shapes, but it is not known if these same theories can be

---

[1]Title, Unclassified.

[2]Presented at NASA Conference on Hypersonic Aircraft Technology, Ames Research Center, May 16-18, 1967.

combined to predict the characteristics of complex multiple-shock systems such as those associated with aircraft-type configurations.

The objectives of this paper are to present experimental aerodynamic characteristics for three representative hypersonic cruise configurations and to compare the results with theoretical estimates.

SYMBOLS

$\bar{c}$	mean aerodynamic chord
C_D	drag coefficient
C_{D_o}	drag at zero lift
C_L	lift coefficient
C_{L_o}	lift at zero angle of attack
C_{L_α}	lift-curve slope
C_{m_o}	pitching-moment coefficient at zero lift
$\left(\frac{L}{D}\right)_{max}$	maximum lift-drag ratio
M	Mach number
S_{ref}	reference wing area
S_v	exposed vertical-tail area
α	angle of attack

EXPERIMENT

Models

The three models used in the present investigations are shown in figure 1. They were designed to the same specifications, namely, an air-breathing, liquid-hydrogen fueled, hypersonic aircraft having a gross weight of approximately a half-million pounds, a cruise Mach number near 6, and a wing area of 6250 square feet. The wings, with an aspect ratio of 1.46, had flat undersurfaces for minimizing local flow acceleration and hypersonic boundary-layer expansion ahead of the inlets. The engines were placed on the three configurations so as to avoid jet impingement on the structure downstream of the nacelle exits. The plane containing the wing lower surface passed through the fuselage center line on the three models.

Reference model.- The model at the top of figure 1 was derived from the analytical studies of reference 1. The fuselage had a circular cross section, a fineness ratio of 12, and a Sears-Haack area distribution. The model scale was 1 inch equals 16 feet full scale. The flat-bottomed wing had a 70° sweptback leading edge and a 4-percent-thick wedge-slab-wedge airfoil section with ridge lines on the upper surface at 30 and 70 percent of the local chords. This model could be fitted with either of two vertical tails, both of which had the same planform (i.e., 60° sweptback leading edges and exposed areas equal to one-fourth of the reference wing area) but different airfoil sections. One vertical tail had a 4-percent-thick symmetrical diamond section; the other had an 8-percent-thick wedge section. The latter vertical tail in effect represents the former tail incorporating flare of the surface aft of the ridge line. The external contours of the two-dimensional nacelles, with the inlets located in the wing compression field, simulated a design containing two turboramjet engines per nacelle. For the reference model, constant-area internal ducts were used, but inlet precompression ramps and boundary-layer bypass were not included.

Flat-bottom model.- The model at the lower left in figure 1 is designated the flat-bottom model because of the flat undersurfaces on all model components. The forebody of the flat-bottom fuselage was longitudinally curved upward to the nose but was laterally flat. The 70° sweptback delta wing was tested with 4- and 3-percent-thick airfoil sections which had rounded ridge lines at 35- and 70-percent chord on the upper surface. The nacelle and horizontal stabilizer combination was designed to bypass the boundary layers from the adjacent wing and body surfaces and to draw air from the compression field under the wing in flight. This model also incorporated a pair of wing-mounted flaps conceived to deflect downward in front of the inlets and to afford protection from debris injestion during powered ground operations. Under these conditions, the inlets would draw air from the upper surface of the wing. The exit areas of the nacelles were twice the inlet areas.

Blended model.- The blended model at lower right in figure 1 had a flattened body of elliptical cross section merged to a 3-percent-thick, 80°-65° double delta wing with clipped tips. The elliptical cross sections had a ratio of major to minor axes of 16/9. The nacelles, like those on the flat-bottom model, provided for boundary-layer bypass. By comparison the nacelles on the blended model were mounted farther forward under the wing, with the ramps above rather than below the inlets. The wing had a double-wedge section with inboard and outboard rounded ridge lines at 64-percent chord on the upper surface. The wing extended relatively far aft on this short body for balance between the weight and aerodynamic forces.

Vertical tails and rudders.- The afterbodies of the flat-bottom and blended models were fitted on the center line with similar vertical tails that had symmetrical wedge-slab-wedge sections, 70° sweptback leading edges, and exposed areas equal to one-tenth the wing reference area. These models were also equipped with identical pairs of wing-mounted 70° sweptback fins with wedges simulating deflected rudders. The combined areas of the three vertical surfaces totaled to the same one-fourth of the wing reference area as that of the single large vertical tail on the reference model.

[redacted]

Tests

Experimental data were obtained in the Ames 6- by 6-foot transonic, 1- by 3-foot supersonic, and 3.5-foot hypersonic wind tunnels over a Mach number range from 0.65 to 7.4. In the 6- by 6-foot tunnel, the Mach number was varied from 0.65 to 2.0 (a few measurements were also made at 0.25), and in the 1- by 3-foot facility, from 2.0 to 4.8. Mach numbers of 5.3 and 7.4 were obtained in the 3.5-foot hypersonic tunnel, where the stagnation temperature was maintained at 800° F to prevent liquefaction of air in the test section. Data were taken at a constant Reynolds number of 3.5 million per foot at all Mach numbers, except 2.0 in the 6- by 6-foot tunnel, where the Reynolds number was held at 2.5 million per foot because of pressure limitations.

The models were sting-mounted through the rear of the fuselages. Force and moment measurements were made with an internally mounted six-component strain-gage balance over a nominal angle-of-attack range from -4° to +12° and angle-of-sideslip range from -2° to +10°. The angles of attack and sideslip were corrected for balance and sting deflections due to the aerodynamic loads, and the measured forces were adjusted to a condition of free-stream static pressure over the model bases.

At several points throughout the test Mach number range, pressure surveys were made of the flow through the nacelles, and the computed results were used to correct for internal drag. Also, the pressure on the base of the reference model nacelles was measured and the axial force adjusted to a condition corresponding to free-stream static pressure.

Generally transition was not fixed on the models, but grit studies were conducted at several of the lower Mach numbers in order to provide an all-turbulent boundary layer as a basis for data evaluation. At the hypersonic speeds, no effective method was found for fixing transition near the leading edges of the model components to achieve fully turbulent flow. Studies utilizing flow visualization and Reynolds number variation indicated the hypersonic boundary layers to be nearly all laminar with possible small areas of transitional flow.

DISCUSSION

Part I - Lift and Drag

This part of the discussion concerns the lift and drag characteristics of the three representative hypersonic cruise configurations. Experimental data obtained for the three models during the wind-tunnel tests are compared over the test Mach number range. The results of several theoretical prediction techniques are correlated with the experimental data for the reference configuration.

Experimental lift and drag.- In order to compare experimental lift and drag characteristics of the three models, it was desired to have the configurations on as nearly an equal basis as possible. Therefore, the comparisons

[redacted]

are made for the wing-body configurations with the vertical tail at the center line but with the nacelles removed. Also, the data as presented are for mixed-flow boundary-layer conditions. The experimental results, indicating very little difference in the lift and drag characteristics of these three configurations throughout the test Mach number range, are presented in figure 2. This figure shows zero-lift drag (C_{D_0}), lift-curve slope at zero lift (C_{L_α}), and untrimmed, maximum lift-drag ratio ($(L/D)_{max}$) versus Mach number for the three models. As can be seen, the nearly identical values of maximum lift-drag ratio decrease from about 9 at 0.9 Mach number to about 4.2 at $M = 6$. Because the experimental results for the three configurations are very similar over the Mach number range, the reference configuration is considered representative for the theoretical comparisons.

Theoretical methods.- Several theoretical prediction methods were employed in a comparison with the foregoing experimental data. A brief summary of these techniques is presented in figure 3. This figure shows the procedures for calculating both pressure and skin friction forces and each has been assigned an identifying number to be used in the figures that follow. Because most of the methods are adequately discussed in the literature, only a brief comment on each will be given here.

In the pressure-force calculation technique number 1, identified as linearized method, the wave drag was computed by a computer program (ref. 2) which applied the supersonic area rule to an "equivalent" body of revolution. The lift characteristics, including wing-body interference effects, and the drag due to wing camber were determined by an aerodynamic influence coefficient program discussed in reference 3. The drag due to lift was set equal to the relation C_L tangent α, which assumes no leading-edge suction or thrust. In the pressure-force calculation procedure number 2, tangent-cone theory was used for the body and tangent-wedge theory for the wing and vertical tail (ref. 4). Pressure-force prediction technique number 3 consisted of Newtonian theory applied to the windward surfaces of the configuration. These latter two theoretical methods employed a Prandtl-Meyer expansion on the leeward or expansion surfaces. Pressure-force prediction methods 2 and 3 did not include the effects of wing-body interference.

The friction drag computation that was combined with the pressure force estimates utilized the reference temperature method of reference 5; in all cases, both an all-turbulent and an all-laminar boundary layer were assumed.

Experiment-theory correlations.- The lift and drag characteristics as computed by the foregoing theoretical methods are compared with the experimental results in the next three figures. These comparisons will be made for the reference model with the nacelles removed.

Zero-lift drag.- The results of correlating the experimental and theoretical zero-lift drag values throughout the test Mach number range are presented in figure 4. This figure is a plot of zero-lift drag (C_{D_0}) versus Mach number. The open symbols denote experimental data for which the boundary-layer flow over the model was mixed, varying from a combination of laminar and turbulent flow at the lower Mach numbers to essentially all-laminar flow at the higher

speeds. The solid symbols represent experimental points for all-turbulent boundary-layer flow. These all-turbulent values were obtained from a detailed wind-tunnel drag study in which six sizes of carborundum particles were used and the grit-free all-turbulent drag level was determined by the methods of reference 6. The linearized method shows excellent agreement with the experimental data for all-turbulent flow at the lower Mach numbers with an error at $M = 1.3$ on the order of 3 percent. However, at Mach numbers above about 4, the drag predictions are too low, since the all-laminar theoretical curve should be approaching the mostly laminar-flow experimental data in this area. Likewise, the drag level predicted by the tangent-cone tangent-wedge theories is low, since, as before, the results of laminar theory should agree closer with the experimental results. Nevertheless, the laminar curve for this theory generally predicts the variation of drag level with Mach number. Hypersonic drag predicted by this theoretical method is too low for several possible reasons, such as model component interference effects, underestimation of the viscous interaction effects, and underestimated contributions of the leeward or "shadow" surfaces. As the figure shows, the Newtonian theoretical estimates are also low in comparison to the data, but this is not unexpected, since, in addition to the aforementioned reasons, the most general application of this theory is for blunt shapes at high hypersonic speeds.

Lift.- In general, the lift characteristics of this type of configuration can be predicted with more certainty than the drag level. This fact is demonstrated in figure 5 which presents a correlation of the theoretical and experimental lift results. The figure is a plot of lift at zero angle of attack (C_{L_0}) and lift-curve slope at zero lift (C_{L_α}) as a function of Mach number. The experimental data indicate that the positive values of lift at zero angle of attack begin to decrease with increasing Mach number until at Mach numbers above about 3 (where the wing leading edge becomes supersonic) the values become slightly negative. As shown on the figure, the C_{L_0} level is overestimated by the linearized method at Mach numbers below 3, but all methods provide good correlation at the higher Mach numbers. The linearized method gives good estimates of lift-curve slope around $M = 2$, but tends to overestimate this value at a Mach number of 3 and above. Tangent-cone and tangent-wedge theories show good agreement with the experimental values of lift-curve slope; but as would be expected at these Mach numbers, Newtonian theory underestimates this parameter. The value of $4/\beta$ is shown on the figure, and when the wing leading edge is supersonic, it gives surprisingly good results for the lift-curve slope of this configuration despite the presence of the large-volume fuselage. With the exception of the Newtonian method, the generally good agreement of the various theories with the experimental data throughout the test Mach number range is evident.

Maximum lift-drag ratio.- Figure 6 presents a correlation of theoretical and experimental values of maximum, untrimmed, lift-drag ratio ($(L/D)_{max}$) as a function of Mach number. As in the case of the drag comparison, the all-turbulent theoretical results of the linearized method exhibit excellent agreement at the lower Mach numbers with the corresponding all-turbulent experimental data, differing only about 5 percent at $M = 1.3$. However, above about $M = 3$, the linearized method predicts too high a value of L/D since the laminar, and not the turbulent-flow curve, should approach the data in

this area. This is a consequence of the low value of drag and high value of lift-curve slope that was predicted in this region as discussed earlier. These same comments apply to the results of tangent-cone and tangent-wedge theories, since, because of the low drag estimates, the predicted L/D values are also too high. It is only fortuitous that the Newtonian method gives good results in the vicinity of M = 5, because, as previously shown, it underestimates both the drag and the lift-curve slope. At around M = 7, however, the Newtonian method also overestimates the maximum L/D values, since the theory for turbulent flow approaches the data for mostly laminar flow.

DISCUSSION

Part II - Stability and Trim

This part of the discussion examines the aerodynamic stability and trim requirements and the related aerodynamic performance penalties of the present models. The effects on stability of variations in Mach number and in model geometry are shown in the figures in the form of longitudinal and directional aerodynamic center locations. The effects on aerodynamic performance of adding the model components and of achieving longitudinal trim and directional stability appear in the form of maximum lift-drag ratios. All aerodynamic centers were evaluated near maximum lift-drag ratio which occurred at angles of attack between 6° and 9°. Aerodynamic characteristics in each case are given both for the basic wing-body models with a vertical tail on the center line and for the complete models.

Longitudinal aerodynamic center.- The longitudinal aerodynamic centers shown in figure 7 for the models with nacelles and wing fins removed indicate that the most rearward locations occurred around M = 1.1, and the most forward locations resulted at or above M = 4.8. The forward placement of the aerodynamic centers for the blended model relative to those of the other two models is not particularly significant here, but rather is a consequence of the more aft location of the wing on this model and the use of percent mean aerodynamic chord rather than percent body length as the ordinate. For perspective, it may be noted that the 5-percent $\bar{c}$ of the blended model and the 35-percent $\bar{c}$ of the flat-bottom model both correspond to 61 percent of the respective fuselage lengths. A significant point to observe in figure 7 is the large 35-percent $\bar{c}$ travel of the aerodynamic center for the blended model, as indicated by the arrow at the right of the figure. The corresponding travel was 16-percent $\bar{c}$ for the flat-bottom model and 21-percent $\bar{c}$ for the reference model. The large travel for the blended model is believed to result from the increased loadings on the forward strakes of the double delta wing and on the wider forebody at hypersonic Mach numbers.

Longitudinal aerodynamic centers - complete models.- The longitudinal aerodynamic centers for the complete models are shown in figure 8. The additions of the nacelles to the reference model and of the nacelles and wing fins to the flat-bottom and blended models moved the longitudinal aerodynamic centers aft. The overall excursions of aerodynamic center over the Mach number range for the reference and flat-bottom models differed by only a few

percent $\bar{c}$ from those shown in figure 7. Adding the nacelles and wing fins to the blended model, on the other hand, significantly reduced the overall excursion of aerodynamic center from the previous 35-percent $\bar{c}$ (fig. 7) to 22-percent $\bar{c}$. This improvement resulted almost entirely from the shift in hypersonic aerodynamic center from -4-percent (fig. 7) to 10-percent $\bar{c}$ for the complete model.

One approach for dealing with the aerodynamic center travel and the associated stability and control problems is fuel-distribution management, which shifts the aircraft center of gravity to maintain acceptable static margins throughout the speed range. Relying on this recourse through the acceleration phase, the present configurations would operate hypersonically with centers of gravity around 35-percent $\bar{c}$ for the flat-bottom vehicle and around 5-percent $\bar{c}$ for the blended configuration.

Directional aerodynamic center.- Another significant problem during acceleration through the supersonic speed range is the deterioration in directional stability. The directional aerodynamic centers of the models with nacelles and wing-fins off are shown in figure 9. The larger vertical tail of the reference model resulted in the directional aerodynamic centers being 20-percent $\bar{c}$ aft of those of the flat-bottom model with the smaller center line vertical tail. The differences in tail size, however, had little influence on the overall travel of the directional aerodynamic centers, which was in the vicinity of 60-percent $\bar{c}$ for both models. A somewhat smaller travel of 47-percent $\bar{c}$ resulted for the blended model. Because of the reductions in static directional stability at the highest Mach number, the hypersonic directional aerodynamic centers shown in figure 9 were generally forward of the longitudinal aerodynamic centers for the complete models (fig. 8).

Directional aerodynamic centers - complete models.- One of the objectives of the present study was to find means for maintaining hypersonic directional stability. One effort consisted of flaring the large vertical tail of the reference model by means of a cross section shape change from a diamond to a wedge. The total leading-edge wedge angle for both tails was 4.6°. The trailing edge of the wedge tail corresponded to a 4-foot thickness full scale. The results shown in figure 10 indicate that the directional aerodynamic center moved aft from 40 percent for the diamond tail to 50-percent $\bar{c}$ for the wedge tail at 5.3 Mach number, but the aerodynamic centers for both tails shifted considerably forward as Mach number was increased to 7.4. Although not shown in figure 10, the directional stability of the reference model with either tail diminished seriously at angles of attack above 6°. Included on figure 10 are theoretical estimates of the hypersonic aerodynamic center locations derived from tangent-cone theory on the forebody, Prandtl-Meyer expansion on the afterbody, and shock expansion on the vertical tails. These inviscid theoretical estimates are in fair agreement with experiment but indicate less variation with Mach number. A possible explanation is that theory does not account for shielding of the tail by the body shock and boundary layers, thus overestimates tail effectiveness at the higher hypersonic Mach number.

A more effective control over hypersonic directional stability is indicated by the results in figure 11 for the flat-bottom and blended models with the small wing-mounted fins and with rudder flare angles up to 35°. The combined area of these fins was 15 percent of the wing reference area, but only 5.4 percent was flared as rudders. As indicated by the vertical spread of the symbols, rudder flare exercised an increasingly powerful control over directional stability and directional aerodynamic center location as hypersonic Mach number was increased. In addition, the directional stability and the rudder control effectiveness did not deteriorate as angle of attack was increased, because the flared rudders extended below the wings and remained in windward exposure with high local dynamic pressure.

Included on figure 11 are theoretical estimates of the incremental changes in aerodynamic center due to inviscid oblique-shock loadings on the flared rudder surfaces only. The inadequacy of inviscid theory in predicting the effects of increasing hypersonic Mach number results from its not accounting for the additional loading induced on the fin surfaces upstream of the rudder hinge lines, where local separated flows developed and spread chordwise. A theoretical basis is not yet available for estimating these added fin loadings and the locations of separation on the fin and of reattachment on the rudder. The effects of rudder flare on a full-scale vehicle might differ from these model results because of the change in boundary-layer characteristics.

The results in figure 11 indicate that the models were directionally stable for the previously cited center-of-gravity locations (i.e., 35-percent $\bar{c}$ for the flat-bottom model with 25° rudder flare and of 5-percent $\bar{c}$ for the blended model with 15° flare). Rudder flare was effective in offsetting the characteristic nonlinearity of the hypersonic lift curves of the vertical tails wherein reduced slopes prevail at small surface inclination angles. The stabilizer inclination angle, then, is as important at hypersonic speed as is surface area at lower speeds.

Maximum lift-drag ratio.- Flared rudders provided hypersonic directional stability, but the associated drag penalized aerodynamic performance. The maximum lift-drag ratios for the configuration buildup and for various degrees of stability and trim for the flat-bottom and blended models are shown in figures 12 and 13, respectively. The upper curves show the maximum untrimmed lift-drag ratios for the wing-body models with a vertical tail only on the center line. The next curve down in each figure shows the maximum lift-drag ratios for the complete models, untrimmed, with controls neutral. The lowest curves (right triangles) on the left of figures 12 and 13 are the maximum lift-drag ratios for the models longitudinally trimmed and stable for Mach numbers into the supersonic range. The penalty in lift-drag ratio due to longitudinal trimming was directly related to the negative pitching-moment coefficient at zero lift which characterized the effectively cambered, flat-bottomed wings used on the present models. Longitudinal trimming at hypersonic speeds caused no significant penalty in lift-drag ratio, because the pitching moment at zero lift was near zero or positive there. Finally, the lowest curves on the right of each figure (diamonds) show the maximum hypersonic lift-drag ratios for completely stable, trimmed models utilizing rudder flare to achieve directional stability, with centers of gravity at 35-percent $\bar{c}$ for the flat-bottom model and at 5-percent $\bar{c}$ for the blended model. It

is likely that the penalty in lift-drag ratio from flaring the rudders on the flat-bottom model could be halved if the flared rudders were moved from the wing trailing edge to the sides of the aft-mounted nacelle-stabilizer, which would more than double the tail length and would allow a smaller rudder flare angle. The hypersonic maximum lift-drag ratios for both models, trimmed and stable, would be near 3.5.

CONCLUDING REMARKS

An analysis of the experimental aerodynamic characteristics for three models representative of hypersonic cruise aircraft and comparisons with theory have indicated the areas of validity and of inadequacy of various theoretical methods, the prominent stability and trim problems, and the factors affecting aerodynamic performance.

Lift and drag characteristics for the reference model were estimated by a linearized theory, tangent-cone and tangent-wedge approximations, and Newtonian theory, each combined with estimates of all-laminar and all-turbulent skin friction using the reference temperature method, and were compared with experimental results at supersonic and hypersonic Mach numbers up to 7.4. Lift and drag estimates from the linearized method agreed well with experiment for supersonic Mach numbers up to 3. Lift characteristics estimated by the tangent-cone tangent-wedge approach and simple supersonic linear airfoil theory agreed well with experiment at supersonic and hypersonic Mach numbers. Newtonian theory underestimated both the lift and the drag. At Mach numbers above 3, all of the theories underestimated the drag and, therefore, overestimated the lift-drag ratios.

The overall travels of the longitudinal aerodynamic centers were about 20 percent of the wing mean aerodynamic chords, with the hypersonic locations being fairly close to those prevailing at subsonic speeds. Adequate directional stability and control at hypersonic speeds was demonstrated by the use of a pair of wing-mounted fins supporting flared rudders which extended above and below the wing plane. The rudders became increasingly effective in controlling directional stability and directional aerodynamic center location as hypersonic Mach number was increased. Theoretical predictions of stability and control characteristics require further refinement to account for viscous interaction effects which become predominant at the higher hypersonic Mach numbers. The hypersonic maximum lift-drag ratios were above 4.0 untrimmed, decreasing to about 3.5 for the trimmed and stable models that incorporated optimum rudder flare for directional stability.

Ames Research Center
National Aeronautics and Space Administration
Moffett Field, Calif. 94035, May 16, 1967
126-13-03-01-00-21

REFERENCES

1. Gregory, Thomas J.; Petersen, Richard H.; and Wyss, John A.: Performance Trade-Offs and Research Problems for Hypersonic Transports. J. Aircraft, vol. 2, no. 4, 1965, pp. 266-271.

2. Harris, Roy V., Jr.: An Analysis and Correlation of Aircraft Wave Drag. NASA TM X-947, 1964.

3. Woodward, F. A.; and Larson, J. W.: Staff of the Aerodynamic Research Unit. A Method of Optimizing Camber Surfaces for Wing-Body Combinations at Supersonic Speeds. Part I. Theory and Application. DOC. D6-10741, Pt. I (prepared for NASA under contract No. NAS2-2282), The Boeing Co., 1965.

4. Ames Research Staff: Equations, Tables, and Charts for Compressible Flow. NACA TR 1135, 1953.

5. Eckert, E. R. G.: Survey on Heat Transfer at High Speeds. WADC TR 54-70, 1954.

6. Braslow, Albert L.; Hicks, Raymond M.; and Harris, Roy V., Jr.: Use of Grit-Type Boundary-Layer-Transition Trips on Wind-Tunnel Models. NASA TN D-3579, 1966.

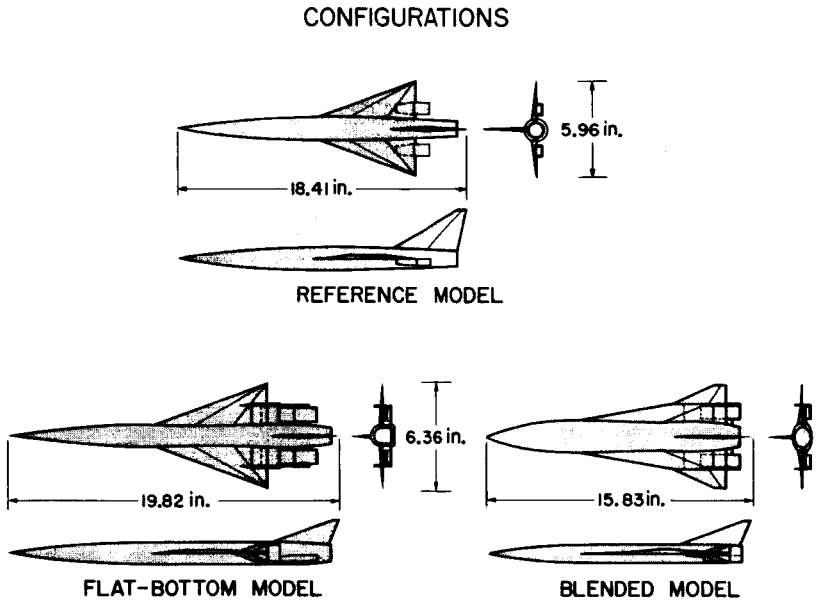

Figure 1

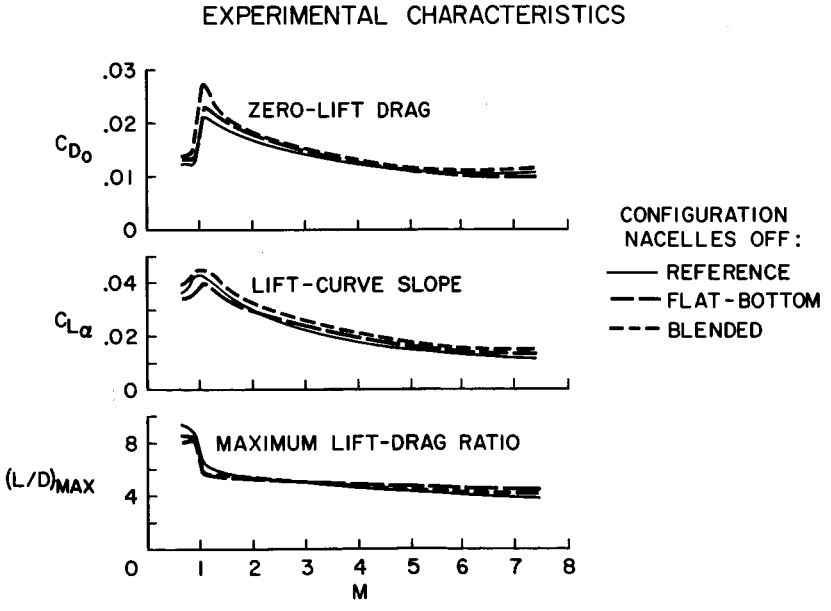

Figure 2

THEORETICAL PREDICTION TECHNIQUES

PRESSURE FORCES	+	SKIN FRICTION
❶ LINEARIZED METHOD	+	REFERENCE TEMPERATURE
❷ TANGENT CONE AND WEDGE	+	REFERENCE TEMPERATURE
❸ NEWTONIAN	+	REFERENCE TEMPERATURE

Figure 3

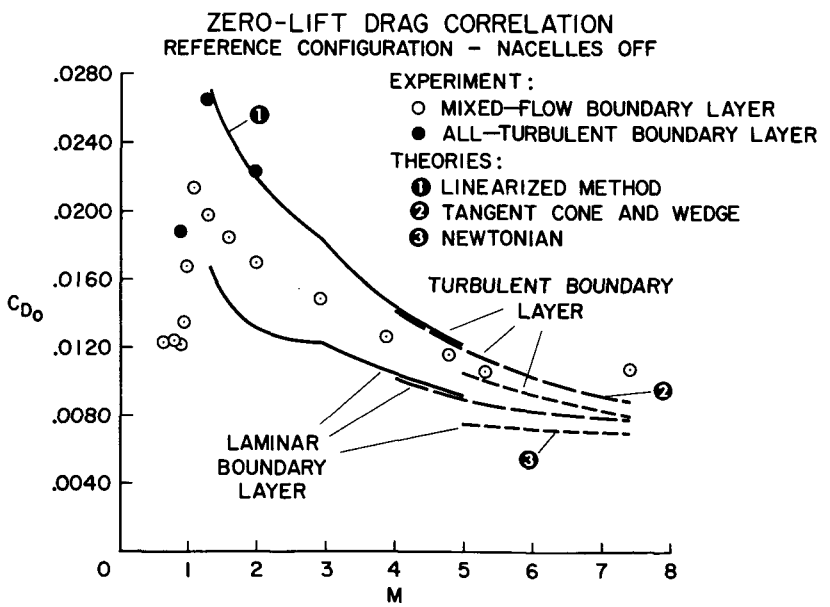

Figure 4

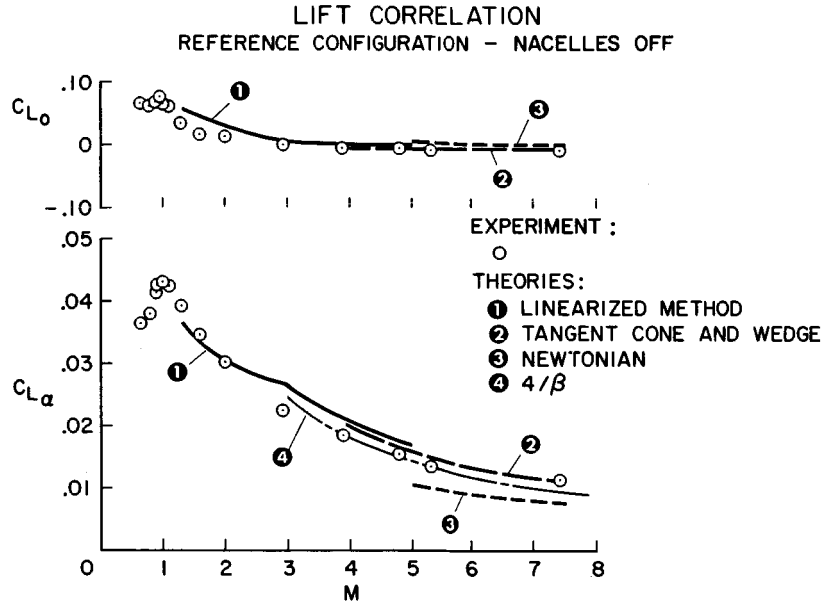

Figure 5

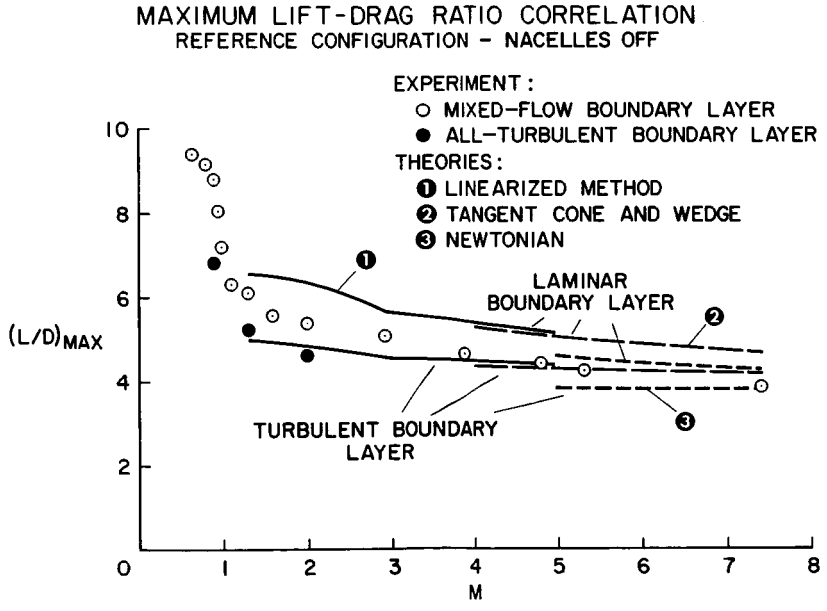

Figure 6

LONGITUDINAL AERODYNAMIC CENTER
NACELLES AND WING FINS OFF

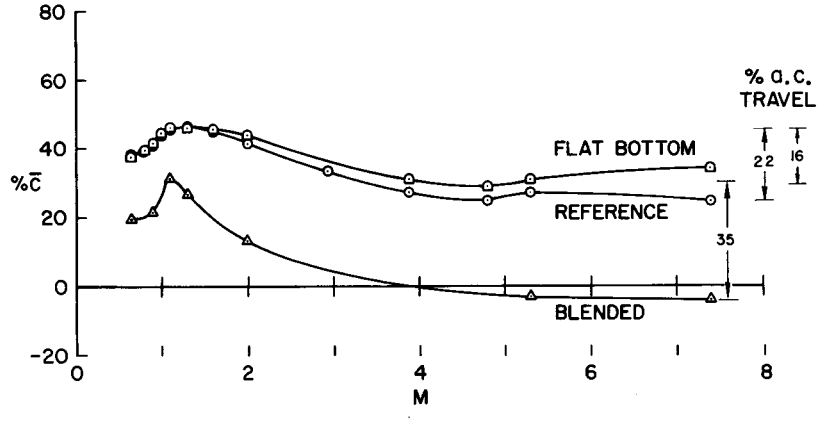

Figure 7

LONGITUDINAL AERODYNAMIC CENTER
COMPLETE MODELS

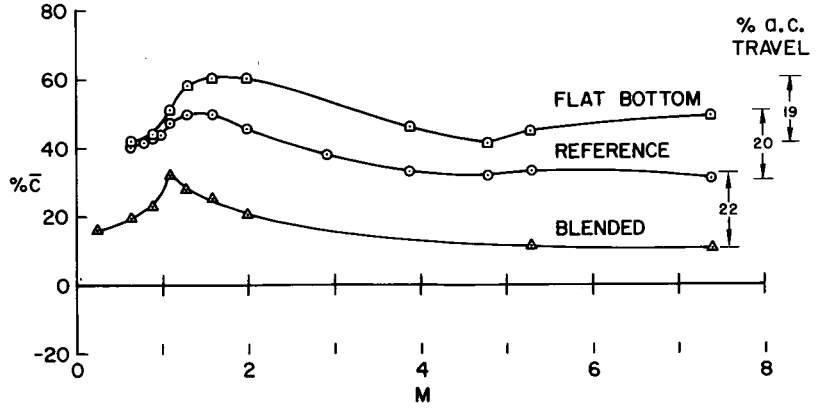

Figure 8

DIRECTIONAL AERODYNAMIC CENTER
NACELLES AND WING FINS OFF

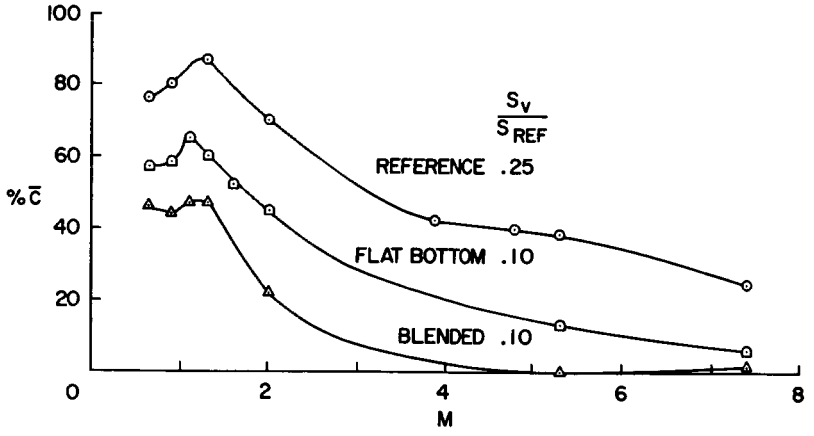

Figure 9

DIRECTIONAL AERODYNAMIC CENTER
REFERENCE MODEL

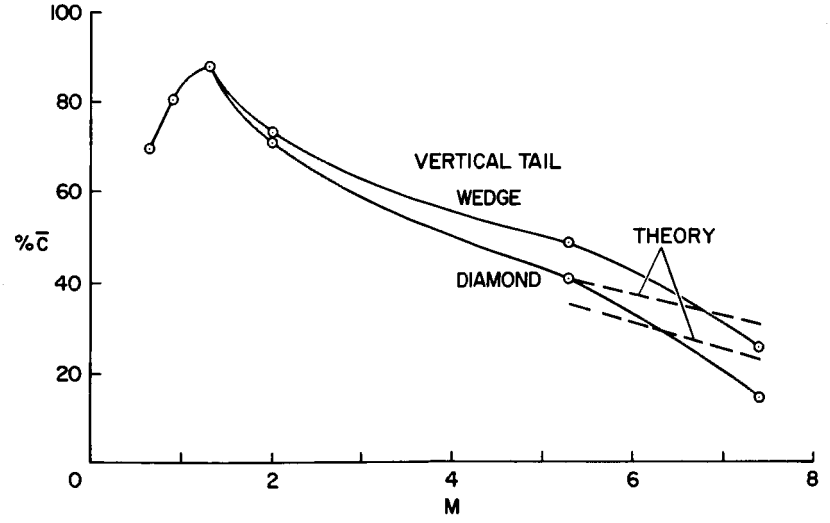

Figure 10

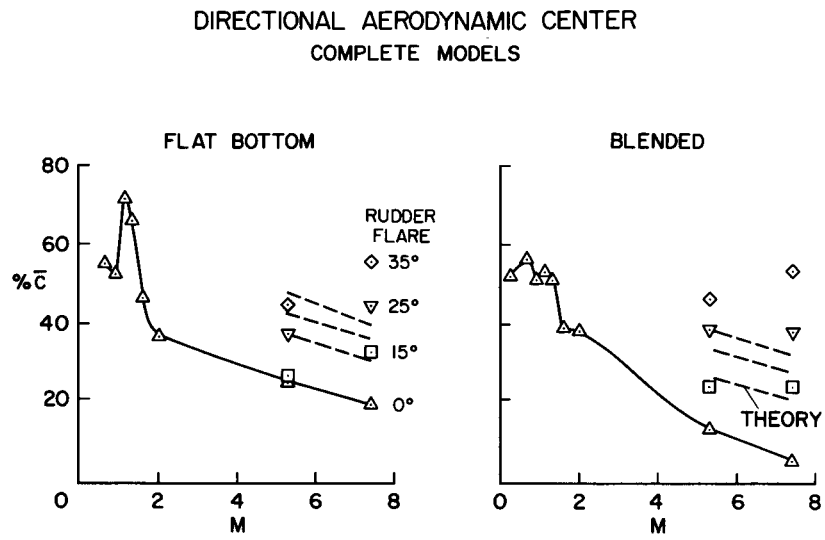

Figure 11

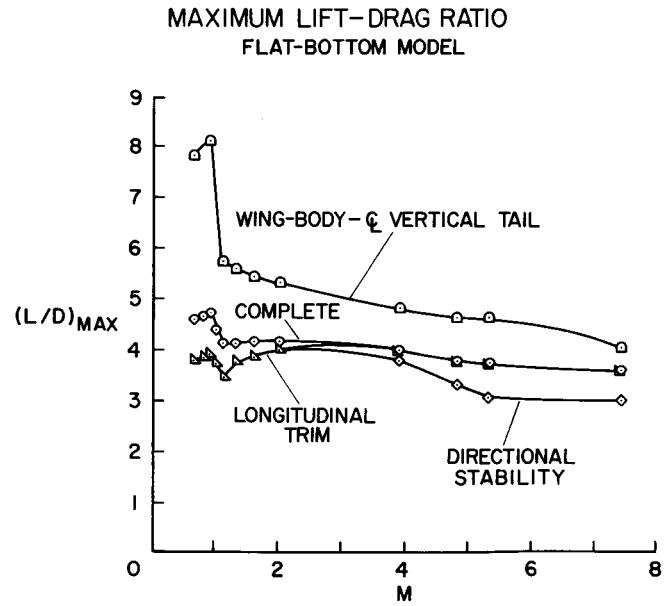

Figure 12

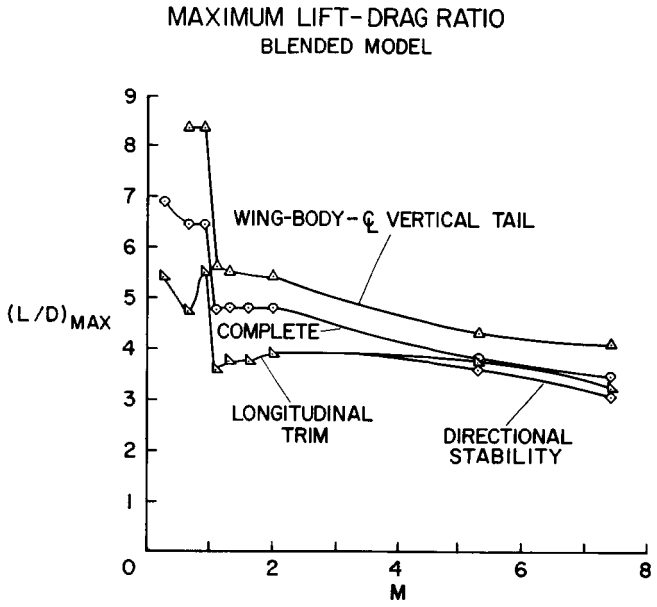
MAXIMUM LIFT-DRAG RATIO
BLENDED MODEL
$(L/D)_{MAX}$
WING-BODY-℄ VERTICAL TAIL
COMPLETE
LONGITUDINAL TRIM
DIRECTIONAL STABILITY
M
0
1
2
3
4
5
6
7
8
9
2
4
6
8

Figure 13